THE JOURNAL OF BIOLOGICAL CHEMISTRY VOL. 289, NO. 19, pp. 13445–13460, May 9, 2014

Syntenin-1 and Ezrin Proteins Link Activated Leukocyte Cell Adhesion Molecule to the Actin Cytoskeleton*

Received for publication, January 2, 2014, and in revised form, March 18, 2014 Published, JBC Papers in Press, March 24, 2014, DOI 10.1074/jbc.M113.546754

Cicerone Tudor[‡§1,2,3], Joost te Riet[¶1,4], Christina Eich[¶5], Rolf Harkes[‡6], Nick Smisdom[‖7], Jessica Bouhuijzen Wenger[§3], Marcel Ameloot[‖8], Matthew Holt[‡3], Johannes S. Kanger[‡], Carl G. Figdor[¶9], Alessandra Cambi[‡¶10], and Vinod Subramaniam[‡11]**

*From the [‡]Nanobiophysics, MIRA Institute for Biomedical Technology and Technical Medicine and MESA+ Institute for Nanotechnology, University of Twente, 7500AE Enschede, The Netherlands, the [§]Laboratory of Glia Biology, VIB Center for the Biology of Disease and KU Leuven Center for Human Genetics, O&N4 Herestraat 49, 3000 Leuven, Belgium, the [¶]Department of Tumor Immunology, Radboud Institute for Molecular Life Sciences, Radboud University Medical Center, 6500HB Nijmegen, The Netherlands, the [‖]Biomedical Research Institute, Hasselt University, Agoralaan Building C, B-3590 Diepenbeek, Belgium, and the **Flemish Institute for Technological Research, Environmental Risk and Health Unit, Boeretang 200, 2400 Mol, Belgium*

Background: The activated leukocyte cell adhesion molecule (ALCAM) is involved in immune responses and cancer metastasis.
Results: ALCAM is linked to the actin cytoskeleton through a supramolecular complex, including ezrin and syntenin-1.
Conclusion: ALCAM supramolecular complex engaged to CD6 stabilizes the immunological synapse.
Significance: Insights into the immunological synapse at the dendritic cell side contribute to clarify immune regulation mechanisms.

Activated leukocyte cell adhesion molecule (ALCAM) is a type I transmembrane protein member of the immunoglobulin superfamily of cell adhesion molecules. Involved in important pathophysiological processes such as the immune response, cancer metastasis, and neuronal development, ALCAM undergoes both homotypic interactions with other ALCAM molecules and heterotypic interactions with the surface receptor CD6 expressed at the T cell surface. Despite biochemical and biophysical evidence of a dynamic association between ALCAM and the actin cytoskeleton, no detailed information is available about how this association occurs at the molecular level. Here, we exploit a combination of complementary microscopy techniques, including FRET detected by fluorescence lifetime imaging microscopy and single-cell force spectroscopy, and we demonstrate the existence of a preformed ligand-independent supramolecular complex where ALCAM stably interacts with actin by binding to syntenin-1 and ezrin. Interaction with the ligand CD6 further enhances these multiple interactions. Altogether, our results propose a novel biophysical framework to understand the stabilizing role of the ALCAM supramolecular complex engaged to CD6 during dendritic cell-T cell interactions and provide novel information on the molecular players involved in the formation and signaling of the immunological synapse at the dendritic cell side.

The activated leukocyte cell adhesion molecule (ALCAM)[12] is a type I transmembrane protein member of the immunoglobulin superfamily of cell adhesion molecules initially identified in activated leukocytes (1). Later studies have reported ALCAM as being expressed also in monocytes (2), bone marrow stromal cells (3), and hematopoietic supporting osteoblastic cells (4). There is ample evidence in the literature revealing the involvement of ALCAM-mediated interactions in several important physiological processes such as maturation of hematopoietic stem cells in blood forming tissues (3, 5, 6), neural development

* This work was supported in part by the Foundation for Fundamental Research on Matter (to the V. S. laboratory).
[1] Both authors contributed equally to this work.
[2] Supported by grants from the Marie Curie Research Training Network IMMUNANOMAP Grant MRTN CT-2006-035946 (awarded to C. G. F. and V. S.).
[3] Supported by ERC Starting Grant ERC-2011-Stg-281961 (awarded to M. H.).
[4] Supported by an EMBO Short Term Fellowship ASTF 293-2011 and Veni Grant 680-47-421 from The Netherlands Organisation for Scientific Research.
[5] Present address: Erasmus Medical Center, Stem Cell Institute, Dept. of Cell Biology, Dr. Molewaterplein 50, 3000 CA Rotterdam, The Netherlands.
[6] Present address: Leiden Institute of Physics, Leiden University, Niels Bohrweg 2, 2333 CA Leiden, The Netherlands.
[7] Supported by a postdoctoral scholarship of Research Foundation-Flanders (FWO-Vlaanderen).
[8] Recipient of support from the Province of Limburg (Belgium) for support within the tUL IMPULS FASE II program allowing for upgrading the laser source used in this work.
[9] Recipient of a NWO Spinoza Prize and ERC Advanced Grant ERC-2010-AdG-269019.
[10] Recipient of an NWO Meervoud subsidy and European Grant NANOVISTA (ICT-2011.3.5/288263). To whom correspondence may be addressed: Nanobiophysics, MIRA Institute for Biomedical Technology and Technical Medicine and MESA+ Institute for Nanotechnology, University of Twente, Enschede, The Netherlands. Tel.: 31-24-3610556; E-mail: a.cambi@ncmls.ru.nl.
[11] To whom correspondence may be addressed: FOM Institute AMOLF, Science Park 104, 1098XG Amsterdam, The Netherlands. Tel.: 31-20-7547400; E-mail: subramaniam@amolf.nl.

[12] The abbreviations used are: ALCAM, activated leukocyte cell adhesion molecule; APC, antigen-presenting cell; CD, cluster of differentiation; DC, dendritic cell; FLIM, fluorescence lifetime imaging microscopy; ERM, ezrin-radixin-moesin; AFM, atomic force microscopy; SCFS, single-cell force spectroscopy; LatA, latrunculin A; ConA, concanavalin A; RFP, red fluorescent protein; PNS, post-nuclear supernatant; pN, piconewton; WB, Western blot.

(7, 8), the immune response (1), and osteogenesis (9). Furthermore, ALCAM has been associated with the progression of diverse types of cancer such as bladder cancer (10), breast cancer (11, 12), colorectal carcinoma (13), melanoma (14–16), and more recently also glioblastoma (17).

ALCAM mediates homotypic ALCAM-ALCAM adhesion (1, 18, 19) but heterotypic interactions with the T cell antigen CD6 have also been described. In fact, ALCAM is the only known ligand for CD6 identified on immune cells (1, 20) and has been shown to localize at the immunological synapse (21) in an antigen-dependent manner (22). More recently, ALCAM-CD6 interactions have been reported to be involved in leukocyte migration across the blood-brain barrier (23). We previously demonstrated that ALCAM-CD6 engagement plays a pivotal role during early T cell-dendritic cell (DC) contact formation and at later stages of T cell activation (24).

Intravital microscopy studies indicated that, within lymphoid tissue, naive T cells scan the surface of DCs at relative cell speeds of up to 30 μm/min (25). The ability to withstand shear at the molecular level is therefore essential for establishing and maintaining productive DC-T cell contacts for prolonged periods of time. These findings indicate a key role for both homo- and heterotypic ALCAM-mediated adhesion during highly dynamic cellular interactions occurring under different conditions of external loading.

By using single-cell force spectroscopy (SCFS), we previously demonstrated that homo- and heterotypic ALCAM-mediated adhesion is governed by distinct kinetic and mechanical properties and that the ALCAM-CD6 bond is significantly more stable under mechanical stress (26). More specifically, ALCAM-CD6 interactions displayed higher tensile strengths and a significantly smaller reactive compliance, suggesting that this heterotypic bond is more resistant to applied force, and hence more stable under conditions of mechanical stress than the homotypic bond (26).

Interactions between plasma membrane components, signaling molecules, and the actin cytoskeleton are important to coordinate in time and space the signal transduction machinery leading to downstream activation events (27). Whereas numerous studies have addressed the signal transduction events taking place at the T cell side of the immunological synapse, very little is known about the biochemical events triggered at the DC side. A sustained association between ALCAM and actin at the DC side of the immunological synapse could play a role not only in regulating the strength and duration of the cell-cell contact but possibly also in regulating signal transduction into the DCs. Despite biochemical and biophysical evidence of a dynamic association between ALCAM and the actin cytoskeleton (18, 19, 26), no detailed information is available about how this association occurs at the molecular level.

The development of new fluorescent probes together with recent advances in fluorescence microscopy deliver powerful tools to study protein interactions in living cells at the molecular level. Fluorescence resonance energy transfer (FRET) is widely used for quantifying protein-protein interactions in living cells (28). Fluorescence lifetime imaging microscopy (FLIM) serves as an appealing alternative to intensity-based approaches to measure energy transfer. Fluorescence lifetime measurements are independent of changes in excitation intensity or fluorophore concentration. Moreover, spectral bleed through rarely presents a problem in FLIM imaging. When the acceptor molecules are in molecular proximity of the donor (*i.e.* ~5–10 nm), energy transfer occurs, which leads to a decrease in donor fluorescence lifetime. FRET-FLIM is therefore a powerful and well established method to visualize and quantify protein-protein interactions in living cells (29–32).

Interactions between transmembrane proteins like ALCAM and the actin cytoskeleton are usually not direct but rather are mediated by linker molecules that recognize, on the one hand, conserved amino acid sequences present at the cytoplasmic tail of the transmembrane proteins and, on the other hand, bear an actin-binding domain (33). The short cytoplasmic tail of ALCAM does not contain a direct binding site for actin. However, the cytoplasmic tail of ALCAM contains a cluster of positively charged amino acids that resembles known motifs recognized by actin-binding proteins of the ERM family, such as ezrin, moesin, and radixin (34, 35). Moreover, the cytoplasmic domain of ALCAM has a KTEA amino acid motif that represents a characteristic type I PDZ-binding motif (36). This short sequence is known to be recognized by the PDZ domain containing protein syntenin-1, which is also able to link transmembrane proteins to the cortical actin cytoskeleton (22, 37). It remains to be determined whether these actin-binding proteins interact with ALCAM.

In this study, we sought to determine the molecular mechanisms regulating the interaction between ALCAM and the actin cytoskeleton in relation to ALCAM's function as a CD6-binding receptor. By exploiting a combination of complementary microscopy techniques delivering quantitative biophysical information such as FRET-FLIM and single-cell force spectroscopy, we demonstrate the existence of a preformed supramolecular complex where ALCAM stably interacts with actin by binding to syntenin-1 and ezrin. This complex is further strengthened upon ALCAM binding to the ligand CD6. Altogether, our data propose a novel framework to understand the stabilizing role of the ALCAM supramolecular complex engaged to CD6 during DC-T cell interactions.

EXPERIMENTAL PROCEDURES

Materials—Monomeric red fluorescent protein (RFP) was a gift of Dr. T. M. Jovin (Max Planck Institute for Biophysical Chemistry, Göttingen, Germany). The ALCAM-wild type (WT), ALCAM-GFP, ALCAM-GPI, and ALCAM-ΔThr (T556A and T581A) constructs were designed and described previously (18, 19). The chimeric ALCAM-RFP construct was generated by substituting green fluorescent protein (GFP) by RFP from pTagRFP-C (Evrogen, Moscow, Russia) in the pEGFP-N3-ALCAM vector (Clontech) using BamHI and NotI restriction sites. K562 cells were transiently transfected by nucleoporation with an Amaxa Nucleofector (Amaxa, Cologne, Germany) according to the manufacturer's instructions and were cultured for 24 h in 12-well plates prior to use. The plasmids for ezrin-GFP and ezrin-RFP were obtained from Prof. S. Mayor, National Centre for Biological Sciences, Bangalore, India (38). The plasmids for syntenin-1-GFP and syntenin-1-mCherry were obtained from Prof. P. Zimmermann, Department of Human Genetics, KU

Leuven, Belgium. The pmTurquoise2-N1 (39) and mVenus (L68V)-mTurquoise2 were a generous gift from Prof. T. W. J. Gadella (Molecular Cytology, University of Amsterdam). The pN1-mVenus plasmid was created by inserting the mVenus sequence from mVenus (L68V)-mTurquoise2 into a pN1 vector using BglII and AgeI (Promega) restriction enzymes. This vector was used in creating the human syntenin-1-mVenus construct by introducing human syntenin-1 amplified from hsyn1FL-eGFP (forward, 5′-aaaaaacgagatctcgccaccatgtctctctatccatctc-3′, and reverse, 5′-aaaaaaaaccggtggaacctcaggaatggtgtggtcc-3′) using BglII and AgeI (Promega). Ezrin-mVenus was made by introducing ezrin excised from pHJ421 (Addgene 20680) into pN1-Venus using EcoRI and AgeI (Promega). The ALCAM-mTurquoise2 plasmids were created by amplifying both wild type and mutant with forward primer 5′-aaaaaacggaattcccgccaccatggaatccaaggggcc-3′ and for ALCAM-WT with reverse primer 5′-aaaaaagggatccggggcttcagttttgtgattgttttctt-3′ and for ALCAM-ΔThr with reverse primer 5′-aaaaaagggatccggggcttcagctttgtgattgttttctt-3′. Both ALCAM-WT and ALCAM-ΔThr were inserted into pmTurquoise2-N1 using EcoRI and BamHI (Promega). Plasmids amplification was carried out by using an endotoxin-free maxi-kit from Qiagen (catalog no. 12362) and a standard maxi-kit from Promega (catalog no. A2392). The actin cytoskeleton-disrupting drugs cytochalasin D and latrunculin A were obtained from Invitrogen. Phalloidin was purchased from Invitrogen; the anti-syntenin-1 antibody was a polyclonal rabbit anti-human poly-IgG (sc-48742), and the anti-ezrin antibody was a polyclonal goat anti-human poly-IgG (sc-6409), both from Santa Cruz Biotechnology, Inc. The anti-GFP antibody was a mouse anti-GFP (IgG1) from Pierce, and anti-ALCAM antibody was a mouse anti-human monoclonal IgG2a antibody (clone AZN-L50).

Cell Culture and Transfection Assays—The K562 cell line with stable expression of ALCAM-WT, ALCAM-GFP, or ALCAM-ΔThr was cultured as described previously (19, 26). K562 cells were grown in a mixture of 75% RPMI medium and 25% Iscove's modified Dulbecco's medium (Invitrogen) as described previously (18), containing 10% FBS and 1% antibiotics and antimycotics (Invitrogen), at 37 °C, with 5% CO_2 in a humidified atmosphere. The day before transfection, cells were seeded in a 24-well plate at a density of 100,000 cells/well and grown overnight. Transient transfections in K562 and RAW 264.7 cells were performed by using either of the following transfection reagents FuGENE HD (Promega) or Lipofectamine LTX (Invitrogen). The protocols were followed in accordance with the manufacturer's instructions, and the fluorescence was measured 18–24 h post-transfection.

Substrate Coating—CD6-coated surfaces were prepared using a three-step method as already reported (26). First, the glass dishes were incubated for 1 h at 37 °C with 10 μg/ml goat anti-human Fc (Jackson ImmunoResearch, West Grove, PA) in a buffer containing 20 mM Tris-HCl, 150 mM NaCl, 1 mM $CaCl_2$, 2 mM $MgCl_2$, pH 8.0 (TSM). After washing with TSM, the uncovered glass surface was blocked with TSM containing 1% bovine serum albumin (BSA), incubated for 30 min at 37 °C, and again followed by washing with TSM. Finally, the glass surface was incubated with 10 μg/ml recombinant human CD6-Fc (R&D systems, Minneapolis, MN) in TSM.

FLIM Experiments—Frequency domain FLIM experiments on transfected K562 or RAW 264.7 cells were performed using a Nikon TE2000-U inverted wide field microscope and a Lambert Instruments fluorescence attachment (Lambert Instruments, Roden, The Netherlands) for lifetime imaging (40). A light-emitting diode (Lumiled LUXEON III, λ_{max} = 468 nm) modulated at 40 MHz was used to excite GFP. Fluorescence detection was performed by a combination of a modulated (40 MHz) image intensifier (II18MD; Lambert Instruments) and a CCD camera (CCD-1300QD; VDS Vosskühler, Osnabrück, Germany) with 640 × 512 pixels. The emission of GFP was detected through a narrow emission filter (520/35 nm; Semrock, Rochester, NY) to suppress any fluorescence emission from RFP. Frequency domain FLIM measurements were referenced to a 10 μM solution of rhodamine 6G, the lifetime of which was independently measured by time-correlated single photon counting as 3.94 ns (data not shown). Fluorescence lifetimes were calculated from several regions of interest and defined to include multiple cells, and data are presented as histograms. The fluorescence lifetime histograms were fitted to Gaussian functions, from which the centers of the distributions and the distribution widths were extracted; the errors reported are one-half of the distribution width. For acceptor photobleaching measurements, a USH-102DH 100-watt mercury lamp (Nikon) was used to illuminate the sample for about 5–10 min, yielding ~95% photobleaching. Images were recorded on a cooled CCD camera (Coolsnap HQ, Roper Scientific). 470/22-nm bandpass excitation filter, 495 nm long pass dichroic, and 520/35 nm bandpass emission filters were used for GFP imaging. 530/40-nm bandpass excitation filter, 562 nm long pass dichroic, and 612/23 nm bandpass emission filters were used for RFP photobleaching. Time domain FLIM was performed using a confocal laser-scanning microscope (Zeiss LSM 510 META installed on a Zeiss Axiovert 200 M; Carl Zeiss, Jena, Germany). A pulsed Titanium:Sapphire laser (Mai Tai Deep See, Spectra Physics, Newport Corp.) tuned at 820 nm was used for two-photon excitation. The excitation light was directed to the sample through a water immersion objective (LD C-Apochromat 40×/1.1 W Korr UV-VIS-IR, Zeiss). The emission light was separated from the excitation light using a 735-nm dichroic beam splitter and further filtered using a short pass 735-nm filter, a dichroic beam splitter at FT490, and an BP440–485-nm band pass filter. Finally, a GaAsP detector (H7429-40, Hamamatsu) connected to a Becker and Hickl SPC830 card (Becker and Hickl GmbH, Berlin, Germany) was used to detect the emission light, allowing for time-correlated single photon counting. The fluorescence lifetime images were processed using SPCImage software from Becker and Hickl using the incomplete exponentials model. The quality of the fit was judged by the reduced χ^2 values. For the majority of the pixels, the reduced χ^2 value was smaller than 1.2.

Confocal Microscopy Experiments—To determine co-localization between ALCAM and its interacting partners, cells were either labeled with specific antibodies or transfected with fluorescently tagged proteins. For co-capping experiments, we treated the cells as already reported (41). Briefly, K562 cells expressing the different ALCAM constructs were stained at 4 °C with 10 μg/ml anti-ALCAM mAb AZN-L50. Isotype-spe-

cific controls were always included. Patching was induced by incubation at 12 °C for 1 h, followed by fixation with 2% paraformaldehyde. Subsequently, cells were intracellularly stained by phalloidin-Alexa546 for actin, rabbit poly-IgG anti-syntenin-1 (sc-48742; Santa Cruz Biotechnology), or goat poly-IgG anti-ezrin (sc-6409; Santa Cruz Biotechnology) using 5-min 0.1% Triton in PBS prior to labeling. Cells were mounted onto poly-L-lysine-coated glass coverslips. Cells were analyzed by a Leica confocal laser scanning microscope TCS SP5 II (Leica, Mannheim, Germany) using sequential signal collection to avoid bleed through. Co-localization of ALCAM with actin, syntenin-1, or ezrin was determined by calculating the Manders' correlation coefficients M1 (0 = no co-localization and 1 = 100% co-localization) with the ImageJ (rsb.info.nih.gov) plug-in JACoP (42).

Co-immunoprecipitation Experiments—K562 cells were transfected with a Neon® transfection system (Invitrogen) according to the manufacturer's instructions. Briefly, K562-ALCAM cells were transfected at a ratio of 3 μg of DNA of the reporter construct syntenin-1-GFP to 1×10^7 cells. Transfected K562 cells were lysed in Tris/Triton lysis buffer (10 mM Tris-HCl, pH 7.4, 100 mM NaCl, 1% Triton X-100, 1 mM EDTA, 1 mM EGTA, 10% glycerol, 0.1% SDS, 0.5% sodium deoxycholate) containing EDTA-free protease inhibitor and PhosSTOP (Roche Applied Science). Proteins were separated by SDS-PAGE and transferred to PVDF membranes (Millipore). Subsequently, blots were labeled by mouse anti-ALCAM, rabbit anti-syntenin-1, goat anti-ezrin, or mouse anti-GFP, and scanned by an Odyssey imager (LI-COR Biosciences). Secondary antibodies (LI-COR) used for the immunoblot are as follows: goat anti-rabbit IRDye800 (for syntenin-1); donkey anti-goat IRDye800 (for ezrin); goat anti-mouse IRDye680 (for ALCAM on syntenin-1 WB and for GFP); and donkey anti-mouse IRDye680 (for ALCAM on ezrin WB). ALCAM was enriched from the post-nuclear supernatant (PNS) pre-cleared by protein G-Sepharose 4 Fast Flow beads (GE Healthcare) coated with isotype antibody (IgG2a) and subsequent immunoprecipitation using beads coated with anti-ALCAM (AZN-L50).

AFM-SCFS Measurements—Cells were attached to tipless AFM cantilevers (MLCT-O10, Bruker, Santa Barbara, CA) by concanavalin A (ConA)-mediated linkages as described (26, 43, 44). In short, ConA-coated cantilevers were prepared as follows. Cantilevers were first cleaned by immersion in 1 M sulfuric acid (Sigma) for 1 h, then thoroughly rinsed with Milli-Q water, ethanol, and subsequently dried in a N_2 flow. Following an overnight incubation at 4 °C in biotinylated BSA (biotin-BSA, 0.5 mg/ml in 100 mM $NaHCO_3$, pH 8.6) the cantilevers were rinsed using PBS and exposed to 0.5 mg/ml (PBS, 30 min, 37 °C) streptavidin (Pierce). Finally, the cantilevers were rinsed three times with TSM and incubated in biotinylated ConA (biotin-ConA, 0.4 mg/ml in TSM) for 30 min at 37 °C and washed with TSM. Force measurements on living cells were performed in force-distance mode using a combined BioScope Catalyst AFM (Bruker) mounted on a Leica TCS SP5 II confocal microscope. Cantilever deflection was determined from the difference in signal generated by a two-segment photodiode monitoring the reflection of a laser beam focused onto the apex of the cantilever. The spring constant of each cantilever was calibrated before use by a nondestructive thermal oscillation method (45). For AFM cell adhesion measurements ($n \geq 7$ cells), a cell was first adhered to the cantilever. The cantilever was pushed softly (<3 nN) onto the cell for ~10 s, and upon retraction, a positive pickup was directly observed by the microscope. From that moment, the cell was allowed to adhere strongly to the cantilever for at least 10 min. Adhesion of the cantilever-adhered cell to CD6-Fc-coated glass substrates (50-mm glass bottom Petri dishes, WillCo Wells BV, Amsterdam, The Netherlands) was subsequently measured by bringing the cell into contact with the substrate with a contact force of 1 nN and allowing the cell to adhere for 2 s. Subsequently, the cell was retracted at a retraction speed at 12 μm/s, with subsequently a relaxing time of 10 s to give the cell time to recover (43). Cell adhesion experiments were performed in a perfusion chamber at 37 °C. Data were exported from the BioScope Catalyst by the NanoScope Version 8.1 software and further analyzed in MATLAB. Analysis of force-distance curves resulted in the maximum detachment force F_{max} of every curve.

RESULTS

Analysis of ALCAM Interaction with the Actin Cytoskeleton by Fluorescence Lifetime Imaging Microscopy—Previous work from our laboratories demonstrated a role for the actin cytoskeleton in ALCAM-mediated adhesion by using both biophysical and biochemical approaches (18, 26). To confirm this interaction by FLIM, we used K562 cells stably expressing ALCAM-GFP and transfected with RFP-tagged actin. Inspection by confocal microscopy showed good expression levels of plasma membrane localized ALCAM and intracellular actin and confirmed their co-localization already prior to engagement of ALCAM with its ligand (Fig. 1*A*). Subsequently, K562 cells co-expressing ALCAM-GFP and actin-RFP were subjected to FRET-FLIM analysis (Fig. 1, *B* and *C*). The lifetimes of the donor (GFP) for several individual cells in a field of view were calculated from frequency domain FLIM images, and fluorescence lifetime histograms were obtained. After Gaussian fitting of the histograms, the average GFP lifetime of K562 cells expressing ALCAM-GFP only was found to be 2.89 ± 0.23 ns and was unaltered upon co-expression of cytosolic RFP. In contrast, in K562 cells expressing both ALCAM-GFP and actin-RFP, the average fluorescence lifetime for GFP was 2.73 ± 0.17 ns; this decrease in fluorescence lifetime relative to the control values suggested a physical proximity between ALCAM and actin (Fig. 1*C*). Selective photobleaching of the acceptor (RFP) under the same conditions showed a complete recovery of the GFP lifetime (2.82 ± 0.17 ns) (Fig. 1*D*), indicating that the decrease in the fluorescence lifetime of ALCAM-GFP in the presence of actin-RFP could be unambiguously attributed to energy transfer between GFP and RFP. These data clearly demonstrate co-localization of ALCAM and actin at the nanometer level and motivate the application of FLIM to further investigate the ALCAM-cytoskeleton interaction at the molecular level.

ALCAM Interacts with Ezrin and Syntenin-1—As depicted in Fig. 2*A*, the cytoplasmic tail of ALCAM contains putative ERM and syntenin-1-binding motifs. To investigate whether these cytoplasmic linker molecules are involved in linking ALCAM to

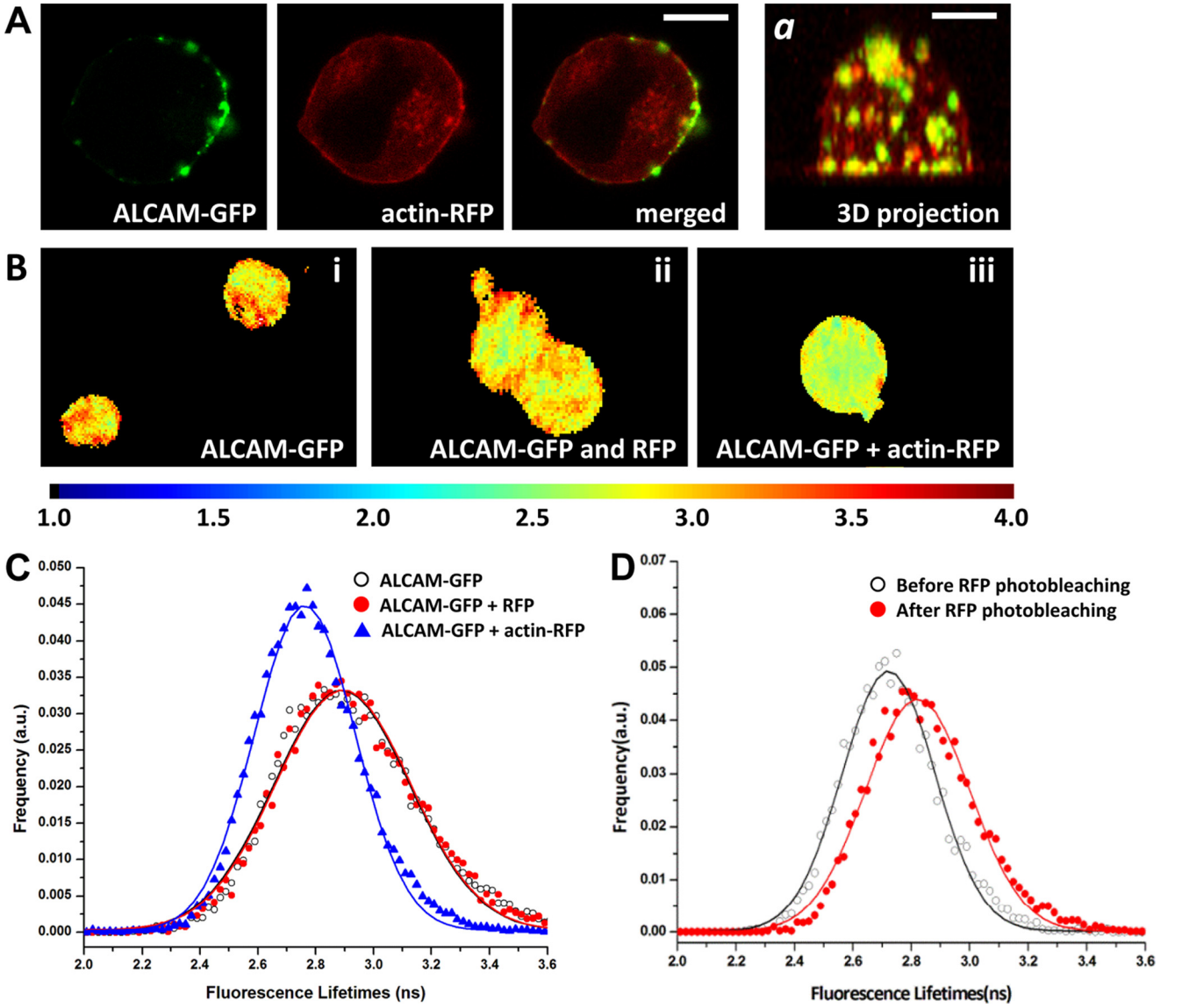

FIGURE 1. **Ligand-independent interaction between ALCAM and actin is detected by FRET-FLIM.** *A,* confocal microscopy shows the co-localization between ALCAM and actin in fixed K562 cells double-transfected with ALCAM-GFP (*green*) and actin-RFP (*red*). *Panel a* represents a merged three-dimensional projection of the ALCAM and actin channels. *Scale bar,* 5 μm. *B,* representative FLIM images of K562 cells expressing ALCAM-GFP alone, ALCAM-GFP and cytoplasmic RFP, and ALCAM-GFP and actin-RFP. *Horizontal bar* indicates a continuous color scale of the GFP lifetime, ranging from 1 to 4 ns. *C,* lifetime histogram represents the distribution of average fluorescence lifetime values of GFP molecules recorded from ~100 cells per condition. *D,* fluorescence lifetimes of ALCAM-GFP co-expressed with actin-RFP were collected from ≈ 6–10 cells (*open symbols*). Subsequently, the acceptor RFP was photobleached, and the average GFP fluorescence lifetime was calculated again (*filled symbols*). *a.u.,* arbitrary units.

the actin cytoskeleton, K562 cells with stable expression of ALCAM-GFP were transiently co-transfected with ezrin-RFP. Donor fluorescence (ALCAM-GFP) lifetime images were collected (Fig. 2*B*), and the FLIM data from over 100 cells were averaged to yield fluorescence lifetime histograms for statistical analyses (Fig. 2*C*). The FLIM images and histograms reveal that the fluorescence lifetime of ALCAM-GFP is decreased in the presence of ezrin-RFP. Gaussian fitting of the histograms resulted in average lifetimes of 2.89 ± 0.23 ns and 2.72 ± 0.19 in the absence and presence of ezrin-RFP, respectively, indicating energy transfer from GFP to RFP and therefore a molecular interaction between ALCAM and ezrin prior to ligand binding. Subsequently, cells co-expressing ALCAM-GFP and ezrin-RFP were allowed to adhere onto glass coverslips previously coated with CD6-Fc, thus stimulating ALCAM-mediated adhesion. The corresponding GFP fluorescence lifetimes were collected, resulting in an average value of 2.64 ± 0.18 ns, indicating that ALCAM-CD6 interactions moderately affect ALCAM-ezrin interactions. Finally, the K562 cells co-expressing ALCAM-GFP and ezrin-RFP on CD6-Fc surfaces were subjected to treatment with LatA, a powerful actin cytoskeleton disrupting agent. The resulting GFP fluorescence lifetimes show fully recovered values of 2.84 ± 0.24 ns, demonstrating that ALCAM-ezrin interactions depend on the integrity of the cortical actin cytoskeleton (Fig. 2*C*). The acceptor photobleaching control further strengthened these observations, with a recovery from 2.62 ± 0.16 to 2.86 ± 0.22 ns after RFP photobleaching (Fig. 2*D*). Treatment with LatA induces a decrease of ALCAM-ezrin co-localization and redistributes ezrin from the membrane cortex to the cytoplasm (Fig. 3). Altogether, these data clearly show

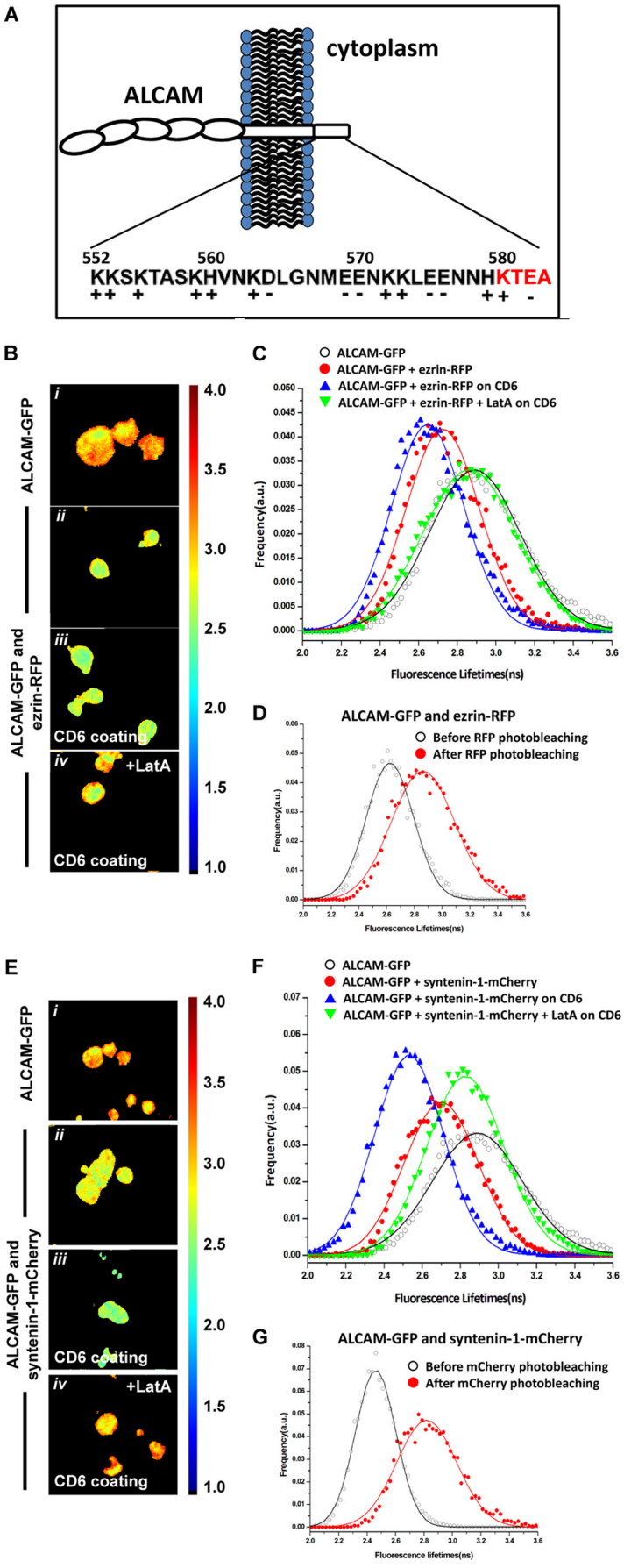

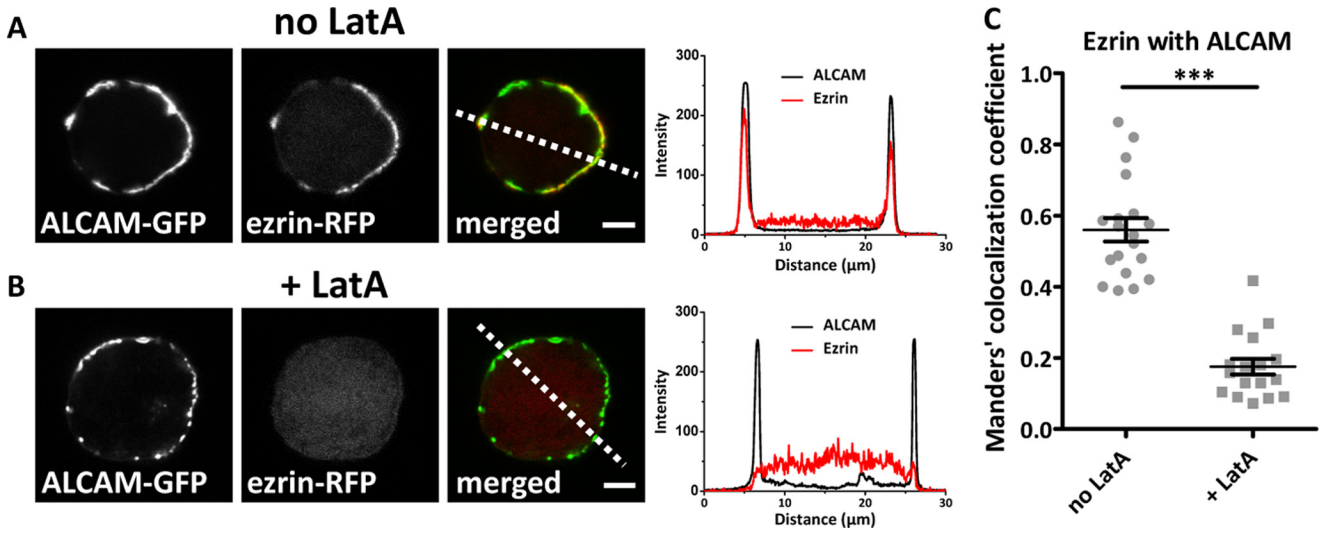

FIGURE 3. **Ezrin localizes to ALCAM only in presence of actin.** *A,* confocal microscopy images of K562 cells double-transfected with ALCAM-GFP and ezrin-RFP show co-localization of ALCAM clusters with ezrin at the cell cortex (*left panels*). Cross-section of the cells indicated show the co-localization of ALCAM and ezrin at the cell cortex (*right panel*). *B,* after treatment of these cells with the actin-disrupting drug LatA for 30 min at 37 °C, co-localization of these ALCAM clusters is disrupted, and ezrin distribution is predominantly cytoplasmic (*left panels*). Cross-section of the cells indicated confirms disruption of co-localization of ALCAM and ezrin and cytoplasmic distribution of ezrin (*right panel*). *C,* quantification of co-localization of ezrin with ALCAM ($n > 15$ cells) by Manders' co-localization coefficient (1 = full co-localization and 0 = none; ***, $p < 0.0001$) with and without LatA treatment.

that ALCAM and ezrin pre-assemble into ligand-independent complexes that are dependent on the intact cortical actin cytoskeleton and that are moderately influenced by ALCAM engagement to its ligand CD6.

Next, we investigated the potential interaction between ALCAM and syntenin-1. K562 cells stably expressing ALCAM-GFP were transiently co-transfected with syntenin-1-mCherry. The mCherry protein is a variant of RFP that also forms a suitable FRET acceptor for GFP. FLIM data of multiple cells were collected (Fig. 2*E*), and the average fluorescence lifetime histogram is shown in Fig. 2*F*. The measurements reveal that the fluorescence lifetimes of ALCAM-GFP are significantly decreased in the presence of syntenin-1-mCherry. Gaussian fitting of the histograms resulted in average lifetimes of 2.89 ± 0.23 and 2.70 ± 0.19 ns in the absence and presence of syntenin-1-mCherry, respectively. Furthermore, cells co-expressing ALCAM-GFP and syntenin-1-mCherry were allowed to adhere onto glass coverslips coated with CD6-Fc. The GFP fluorescence lifetimes were collected, resulting in an average of 2.53 ± 0.16 ns, suggesting a powerful effect of ALCAM-CD6 extracellular binding on enhancing ALCAM-syntenin-1 intracellular interactions, in contrast to the modest effect observed for ALCAM-ezrin interactions. Treatment with LatA leads to a full recovery of the GFP fluorescence lifetimes to 2.82 ± 0.20 ns (Fig. 2*F*). An acceptor photobleaching control also reveals a recovery of GFP fluorescence lifetime from 2.46 ± 0.14 to 2.81 ± 0.21 ns (Fig. 2*G*). To exclude that the interactions observed between ALCAM and ezrin and between ALCAM and syntenin-1 were cell type-specific, analogous FRET-FLIM experiments were performed using antigen-presenting cells, *i.e.* RAW macrophages (Fig. 4, *A* and *B*). These data are similar to those observed on K562 cells (Fig. 2), although LatA treatment with the same concentration appears to have only a partial effect on restoring the lifetime of syntenin-1-GFP on RAW cells, as compared with the more dramatic effect exhibited in K562 cells (Fig. 2*F*). This may be due to the fact that in RAW macrophages the actin cytoskeleton is not fully disrupted. These data demonstrate that in both cell types, syntenin-1 is already present in ligand-independent ALCAM supramolecular assemblies, but ALCAM binding to its ligand CD6 strongly enhances the intracellular interaction between ALCAM and syntenin-1.

To check that our molecules of interest are expressed in primary monocyte-derived DCs, DCs were stained for ALCAM, syntenin-1, and ezrin. Fig. 4*C* shows the co-localization of

FIGURE 2. **ALCAM interacts with ezrin and syntenin-1.** *A,* amino acid sequence of ALCAM cytoplasmic tail. The schematic depicts the cell adhesion molecule ALCAM at the cellular membrane. The short 32-amino acid cytoplasmic tail of ALCAM contains several positively charged amino acids at the juxtamembrane position, which constitute the ERM-binding motif, and the KTEA-binding motif, which is a PDZ-binding site, at the C terminus. *B,* K562 cells expressing ALCAM-GFP were transfected with ezrin-RFP and allowed to adhere onto uncoated coverslips (*panels i* and *ii*) or to coverslips previously coated with CD6-Fc molecules (*panels iii* and *iv*). Cells in *panel iv* were treated with 0.2 μg/ml LatA for 1 h at 37 °C. After 1 h, cells were subjected to FRET-FLIM analysis. *Panels i–iv* are FLIM images of cells from one representative experiment out of at least three. *Vertical bar* indicates a continuous color scale of the GFP lifetime, ranging from 1 to 4 ns. *C,* lifetime histogram represents the distribution of average fluorescence lifetime of GFP molecules recorded from ~100 cells per condition. *D,* fluorescence lifetimes of ALCAM-GFP co-expressed with ezrin-RFP were collected (*open symbols*). Subsequently, the acceptor RFP was photobleached, and the average GFP fluorescence lifetime was calculated again (*filled symbols*). *E,* K562 cells expressing ALCAM-GFP were transfected with syntenin-1-mCherry and allowed to adhere onto uncoated coverslips (*panels i* and *ii*) or to coverslips previously coated with CD6-Fc molecules (*panels iii* and *iv*). Cells in *panel iv* were allowed to adhere to the CD6-coated substrate and subsequently treated with 0.2 μg/ml LatA for 60 min at 37 °C before FRET-FLIM measurements were performed. *Panels i–iv* are representative FLIM images of cells from multiple experiments. *Vertical bar* indicates a continuous color scale of the GFP lifetime, ranging from 1 to 4 ns. *F,* lifetime histogram represents the distribution of average fluorescence lifetime of GFP molecules recorded from ~100 cells per condition. *G,* fluorescence lifetimes of ALCAM-GFP co-expressed with syntenin-1-mCherry were collected (*open symbols*). Subsequently, the acceptor mCherry was photobleached and the average GFP fluorescence lifetime was calculated again (*filled symbols*). *a.u.,* arbitrary units.

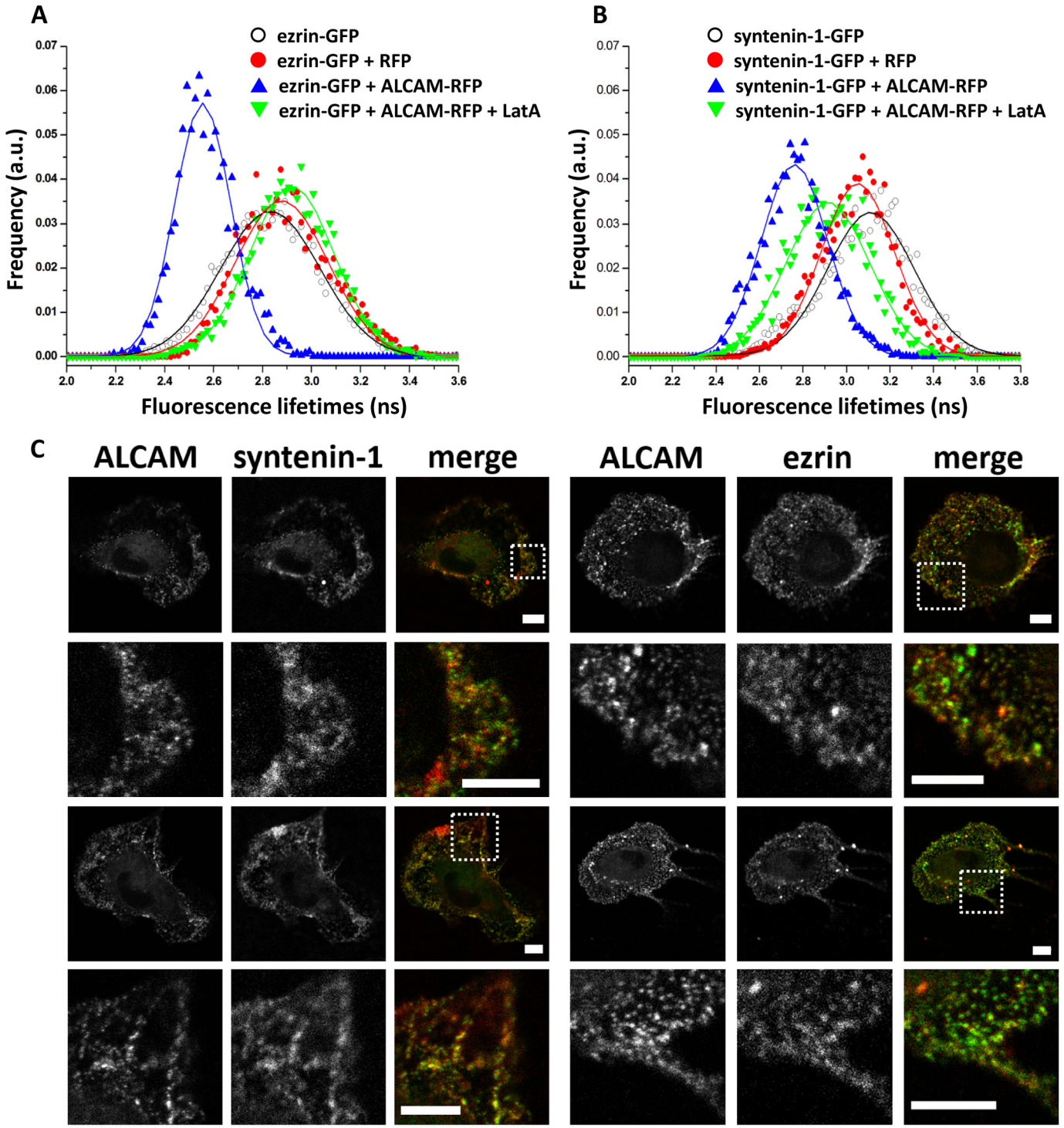

FIGURE 4. **ALCAM interacts with ezrin and syntenin-1 on antigen-presenting cells.** *A,* RAW macrophages were co-transfected with ezrin-GFP and ALCAM-RFP or RFP. Some of the cells were preincubated with 0.2 μg/ml LatA. The lifetime histogram represents the distribution of average fluorescence lifetime of GFP molecules recorded from ~100 cells in the absence/presence of ALCAM-RFP or RFP. *B,* RAW macrophages were co-transfected with syntenin-1-GFP and ALCAM-RFP or RFP. Some of the cells were preincubated with 0.2 μg/ml LatA. The lifetime histogram represents the distribution of average fluorescence lifetime of GFP molecules recorded from ~100 cells in the absence/presence of ALCAM-RFP or RFP. *a.u.,* arbitrary units. *C,* immature monocyte-derived DCs were stained for ALCAM (*green*) and syntenin-1 (*red*) or ALCAM (*green*) and ezrin (*red*) and analyzed by confocal microscopy. Top and third row show two example cells with for each a zoom-in (*dotted lines*) in the rows below. Clusters of co-localized ALCAM and syntenin-1 as well as ALCAM and ezrin are visible at the cell membrane. *Scale bar,* 5 μm.

ALCAM and syntenin-1 as well as of ALCAM and ezrin in small clusters at the cell membrane.

Altogether, these FRET-FLIM data show that both ezrin and syntenin-1 interact with ALCAM's cytoplasmic tail in the absence of ligand binding. Furthermore, although ALCAM-ezrin interaction is only modestly increased by ALCAM binding to CD6, the extent of ALCAM-syntenin-1 interactions is much higher upon the establishment of adhesion, suggesting a different role for these two proteins within the ALCAM supramolecular complex.

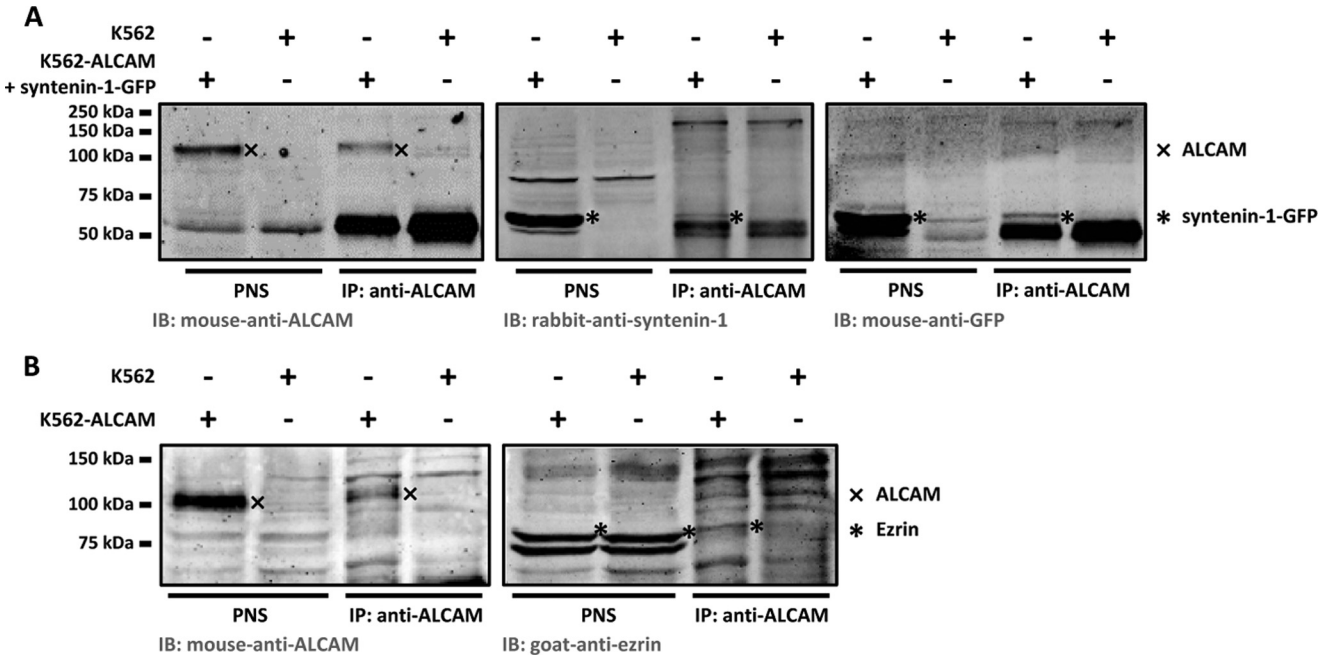

FIGURE 5. **Ezrin and syntenin-1 co-immunoprecipitate with ALCAM.** *A,* ALCAM (expected size ~105 kDa) was detected by mouse anti-ALCAM (AZN-L50) specifically in the PNS of K562-ALCAM cells transfected with syntenin-1-GFP and was absent in the PNS of control K562 cells (*left panel, 1st* and *2nd lanes*). ALCAM was enriched from the PNS of K562-ALCAM + syntenin-1-GFP cells by immunoprecipitation (*IP*) using anti-ALCAM beads (*left panel, 3rd* and *4th lanes*). Syntenin-1-GFP (expected size ~60 kDa) was co-immunoprecipitated with ALCAM only for K562-ALCAM + syntenin-1-GFP cells (*middle panel*). Re-immunoblotting the anti-ALCAM immunoblot (*IB*) with anti-GFP shows that the syntenin-1-GFP bands are specific for syntenin-1 as well as for GFP (*right panel*). *B,* ALCAM was enriched from the PNS of K562-ALCAM cells by immunoprecipitation using anti-ALCAM beads (*left panel*). Endogenous ezrin (expected size ~80 kDa) was co-immunoprecipitated with ALCAM only for K562-ALCAM cells (*right panel*). Endogenous ezrin is also present in the PNS of K562 cells but is not co-immunoprecipitated with ALCAM. Double ezrin bands in PNS are typical for the antibody used.

Syntenin-1 and Ezrin Co-immunoprecipitate with ALCAM—To confirm the interactions of ALCAM with syntenin-1 and ALCAM with ezrin as determined by FLIM, we performed co-immunoprecipitation (co-IP) assays of ALCAM. Syntenin-1 and ezrin were co-immunoprecipitated with anti-ALCAM beads from the PNS of K562 cells stably expressing ALCAM (K562-ALCAM) or PNS of control K562 cells that do not express endogenous ALCAM. We could detect endogenous syntenin-1 by WB; however, the syntenin-1 bands overlapped with unspecific bands probably from the light chain of our immunoprecipitation antibody (data not shown). To circumvent this problem, K562-ALCAM cells were transfected with syntenin-1-GFP. Fig. 5*A* shows that syntenin-1-GFP co-IPs with ALCAM, as detected by a specific antibody recognizing syntenin-1, as well as by an antibody directed against GFP. In addition to syntenin-1, enrichment of ALCAM by a specific immunoprecipitation also showed co-IP of endogenous ezrin, confirming the molecular interaction of ALCAM and ezrin (Fig. 5*B*). Neither syntenin-1-GFP nor ezrin bands could detected in our control immunoprecipitation on non-ALCAM-transfected K562 cells, confirming the specific co-IP of syntenin-1-GFP and ezrin with ALCAM. Thus, taken together, our co-IP and FLIM experiments demonstrate a direct interaction between ALCAM and syntenin-1 as well as ALCAM and ezrin.

Syntenin-1 Interacts with KTEA Sequence of ALCAM—To determine whether syntenin-1 and ezrin are recruited within the same supramolecular assembly that regulates ALCAM-mediated adhesion, we investigated the molecular interaction between these two proteins in the absence and the presence of ALCAM. The K562 cells (mock) as well as K562 cells stably expressing ALCAM wild type (K562-ALCAM-WT) were transiently co-transfected with syntenin-1-GFP and ezrin-RFP, and changes in GFP lifetime were detected by FRET-FLIM analysis. On bare K562 cells, similar GFP fluorescence lifetime values were determined in the absence and in the presence of ezrin-RFP, indicating that in the absence of ALCAM-mediated adhesion, ezrin and syntenin-1 do not interact (Fig. 6*A*). On the contrary, when syntenin-1-GFP and ezrin-RFP were co-transfected in K562-ALCAM-WT cells, a modest decrease in GFP fluorescence lifetime from 2.74 ± 0.16 to 2.61 ± 0.11 ns was observed (Fig. 6*B*). Furthermore, when the K562-ALCAM-WT cells co-expressing syntenin-1-GFP and ezrin-RFP were preincubated with LatA, the GFP fluorescence lifetime value was found to be the same as that observed in K562 cells lacking ALCAM expression (Fig. 6*B*). Finally, both ezrin and syntenin-1 have been confirmed to interact with actin by FLIM measurements (Fig. 6, *D* and *E*). This finding indicates that both ALCAM and an intact actin cytoskeleton are specifically required to form these ligand-independent supramolecular complexes containing ezrin and syntenin-1.

Next, we used K562 cells stably expressing the ALCAM-ΔThr mutant, where the threonine residues at positions 556 and 581 (the latter belonging to the KTEA sequence, the putative binding motif for syntenin-1 (see Fig. 2*A*) (46), were mutated to alanine (19). In particular, the T581A mutation is thought to disrupt the KTEA motif and likely to impair the binding of syntenin-1 to ALCAM. Accordingly, when syntenin-1-GFP was transiently co-transfected with ezrin-RFP in K562 cells stably expressing the ALCAM-ΔThr mutant, no variation in the GFP lifetime values was observed (Fig. 6*C*), indicating

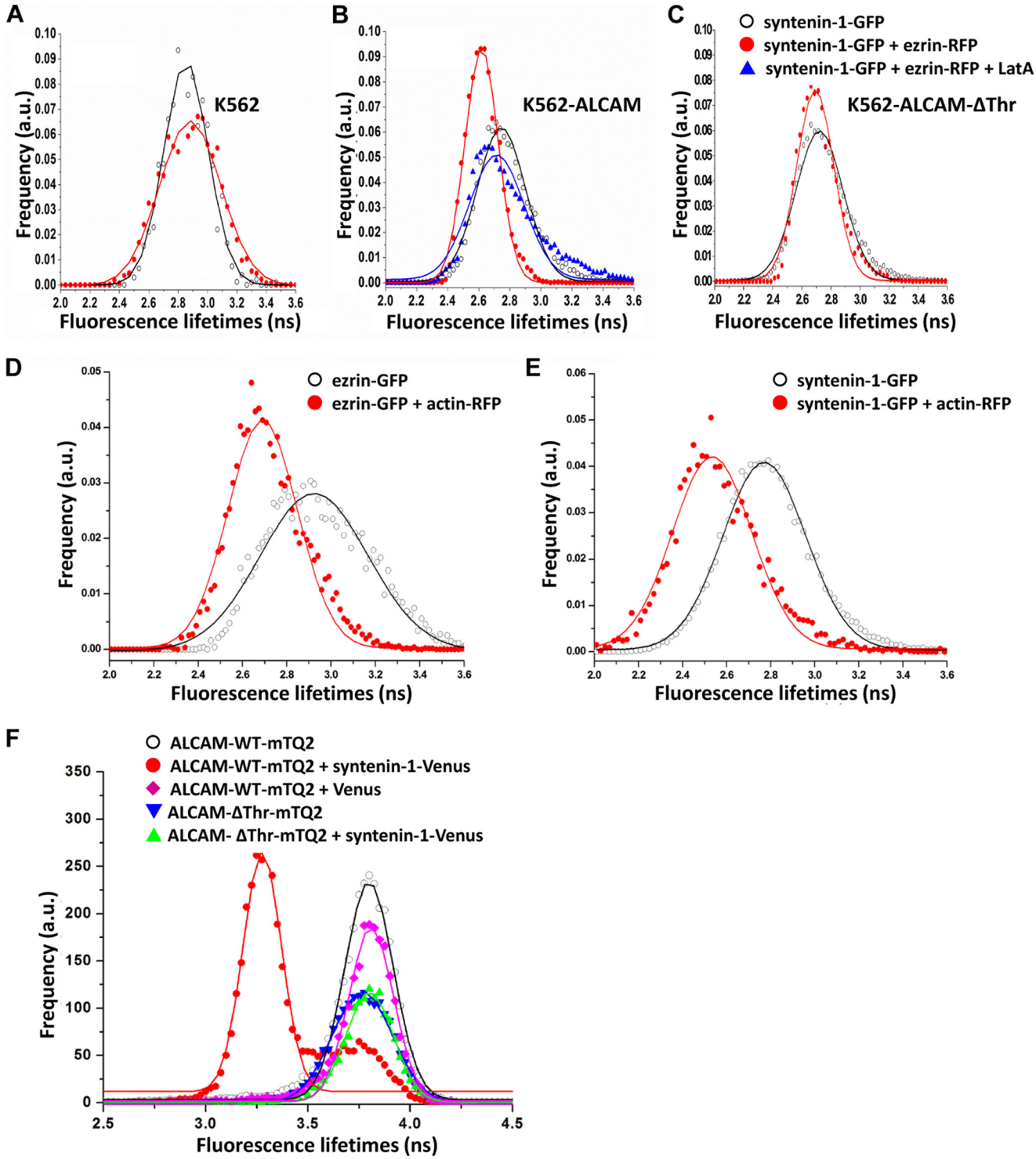

FIGURE 6. **ALCAM specifically recruits ezrin and syntenin-1 to a ligand-independent supramolecular assembly.** Fluorescence lifetime histograms of syntenin-1-GFP co-transfected with or without ezrin-RFP were collected from K562 cells (~100 cells per condition) with no endogenous expression of ALCAM (*A*), from K562-ALCAM-WT cells (*B*), or from K562-ALCAM-ΔThr cells (*C*). *B* also shows the lifetime histogram of syntenin-1-GFP co-transfected with ezrin-RFP, before and after treatment with 0.2 μg/ml LatA. *D*, fluorescence lifetime of K562 cells transfected with ezrin-GFP alone and in combination with actin-RFP (*E*) or with syntenin-1-GFP alone and in combination with actin-RFP clearly indicate molecular scale interactions. *F*, lifetime histograms from K562 cells expressing ALCAM-WT-mTQ2 or ALCAM-ΔThr-mTQ2 co-transfected with syntenin-1-Venus and allowed to adhere onto poly-L-lysine-coated glass bottom dishes for 1 h. The lifetime histogram represents the distribution of averaged fluorescence lifetime of mTQ2 molecules recorded from ~60 cells per condition. *a.u.*, arbitrary units.

that the cytoplasmic tail of ALCAM is essential to recruit syntenin-1 and facilitate its interaction with ezrin. Moreover, FLIM experiments using the FRET pair mTurquoise2 (mTQ2) and Venus (39) on K562 cells transfected with ALCAM-ΔThr-mTQ2 and syntenin-1-Venus confirmed that syntenin-1 can no longer bind ALCAM's cytoplasmic tail in contrast to ALCAM-WT-mTQ2 (Fig. 6*F*). These observations were further supported by the dramatic decrease of co-localization between

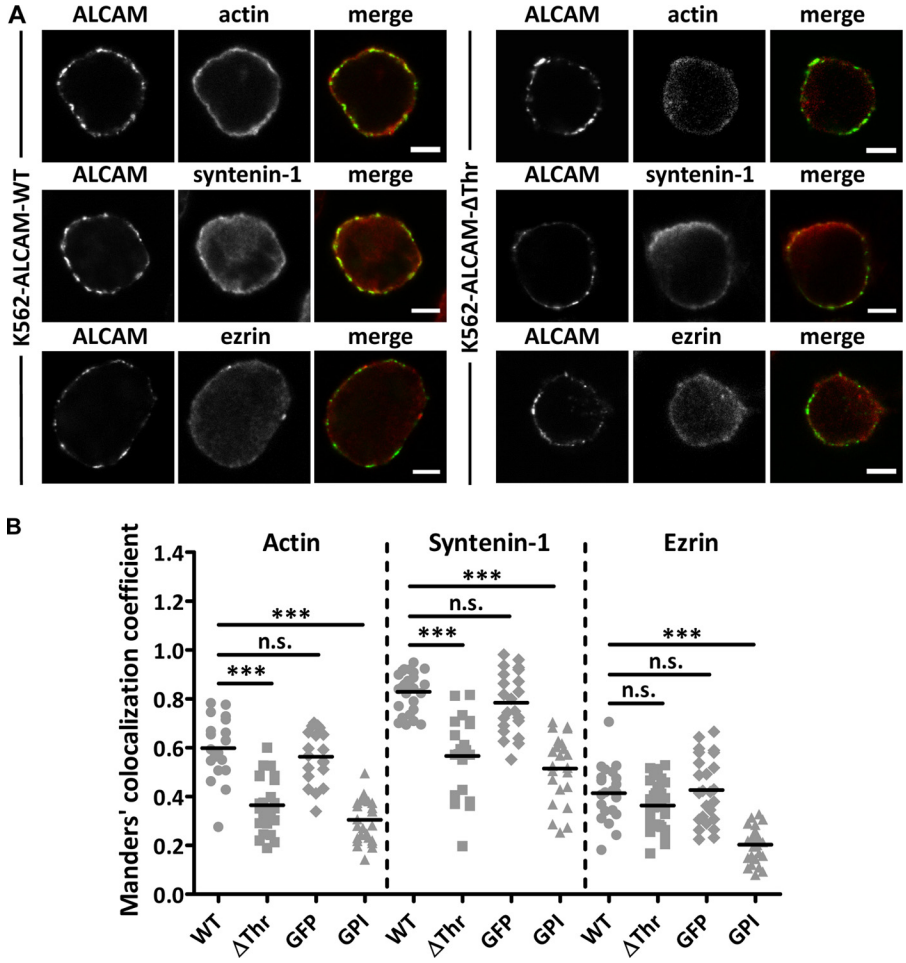

FIGURE 7. **Co-localization of ALCAM with actin, syntenin-1, and ezrin on K562 cells expressing different ALCAM constructs.** *A,* immunofluorescent labeling of actin, syntenin-1, and ezrin on K562-ALCAM-WT and K562-ALCAM-ΔThr cells analyzed by confocal microscopy. Cells were fixed, permeabilized, and co-labeled with antibodies against ALCAM and with either phalloidin to stain actin or with antibodies against syntenin-1 or ezrin. *Scale bars,* 5 μm. Immunofluorescence samples for K562-ALCAM-GFP and K562-ALCAM-GPI are not shown. *B,* quantification of the co-localization between ALCAM and actin, syntenin-1, or ezrin for ALCAM-WT, ALCAM-ΔThr, ALCAM-GFP, and ALCAM-GPI. The GFP tag does not affect ALCAM interactions with cytoskeletal components. When the transmembrane and intracelullar domain of ALCAM are replaced by a GPI anchor, ALCAM cannot interact with any of the cytoskeletal components. Quantification of the co-localization between ALCAM (WT *versus* ΔThr, WT *versus* GFP, and WT *versus* GPI) and actin, syntenin-1, or ezrin was made by calculating the Manders' co-localization coefficient (1 = full co-localization and 0 = no co-localization). *p* values were calculated with the Mann-Whitney statistical test and are indicated in the plot; ***, $p < 0.0001$; *n.s.,* not significant.

ALCAM-ΔThr and actin, or syntenin-1, but not ezrin, as compared with the ALCAM-WT, determined after inducing aggregation of the ALCAM molecules at the cell surface using a specific anti-ALCAM mAb and staining for the cytoskeletal components after fixation and permeabilization of the cells (Fig. 7, *A* and *B*). The presence of a GFP fused to the C terminus of ALCAM did not affect the degree of co-localization with actin, syntenin-1, or ezrin (Fig. 7*B*). In addition, replacing the intracellular and transmembrane domains of ALCAM by a GPI anchor showed that ALCAM cannot interact with any of the intracellular molecules actin, syntenin-1, or ezrin (Fig. 7*B*).

Single-cell Force Spectroscopy Shows Strengthening by Actin Binding—To determine whether syntenin-1 plays a role in ALCAM-mediated adhesion, AFM-based SCFS studies were performed. Similar to earlier studies (26), single K562 cells either expressing ALCAM-WT or the ALCAM-ΔThr mutant were attached to a tipless AFM cantilever by means of ConA-mediated linkages. Subsequently, cell adhesion forces were measured by bringing the ALCAM-expressing K562 cells shortly into contact with CD6-coated substrates before pulling the adhering cells from the substrate (Fig. 8*A*). Repetitive adhesion-detachment cycles, as plotted in so-called force-distance (*F-D*) curves, give information on the strength of the adhesion (Fig. 8*B*). The maximum force (F_{max}) needed to detach the cell from the substrate, derived from the distance between the maximum and baseline of the detachment curve, was taken as a measure for overall cell adhesion (26, 44). After the initial acquisition of *F-D* curves, K562-ALCAM-WT as well as K562-ALCAM-ΔThr cells were blocked *in situ* with the anti-ALCAM mAb AZN-L50 and re-examined under identical experimental conditions (Fig. 8*C*). AZN-L50 specifically blocked 45 ± 6 or 66 ± 7% for ALCAM-WT and ALCAM-ΔThr, respectively, of the total adhesion indicating that the interactions probed are predominantly ALCAM-CD6-mediated (Fig. 8*D*). Comparison of the F_{max} needed to detach the ALCAM-WT and ALCAM-ΔThr cells after a 2-s interaction with CD6 showed that significantly more force (1.45 ± 0.37 *versus* 0.76 ± 0.35 nN) is needed to detach the ALCAM-WT than for the ALCAM-ΔThr-ex-

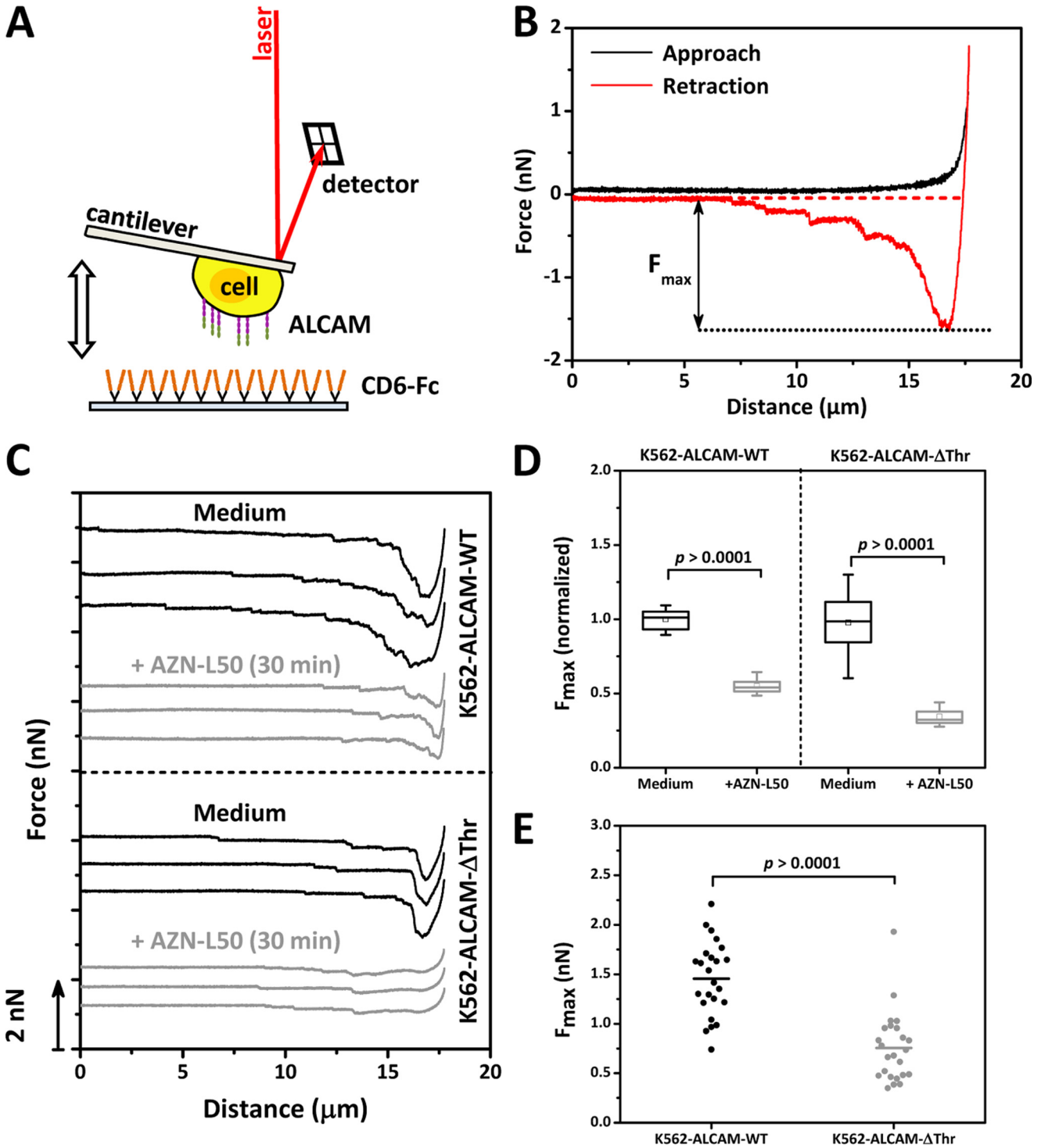

FIGURE 8. **Syntenin-1 recruitment to the supramolecular assembly stabilizes ALCAM adhesion.** *A,* schematic overview of single-cell force spectroscopy measurements. The tipless cantilever with an adhered K562-ALCAM-WT or K562-ALCAM-ΔThr cell was approached toward a surface coated with CD6-Fc. When a contact force of 1 nN was reached, the cell was allowed to adhere for 2 s to the substrate. Then, the cell-functionalized cantilever was retracted from the substrate thereby disrupting the adhesion. When the cell was completely detached, the probing cycle was repeated. *B,* example of a force-distance curve showing the approach and retraction curve and the maximum detachment force (F_{max}), which is the distance between the maximum force and the baseline in the retraction curve. *C,* three representative *F-D* curves displaying the unbinding of K562-ALCAM-WT and K562-ALCAM-ΔThr cells after a 2-s contact with the CD6-Fc-coated substrate. Furthermore, three *F-D* curves are shown after a specificity block with 10 μg/ml of the anti-ALCAM antibody AZN-L50 for 30 min at 37 °C in both the case of K562-ALCAM-WT and K562-ALCAM-ΔThr cells. *D,* box plot showing the specific block ($n = 3$ independent experiments) of the normalized F_{max} of ALCAM-CD6-mediated interactions by the mAb AZN-L50. *E,* scatterplot comparison of F_{max} needed to detach a K562-ALCAM-WT or K562-ALCAM-ΔThr cell ($n = 7$) from a CD6-Fc-coated substrate. Data presented are of $n = 24$ K562-ALCAM-WT and K562-ALCAM-ΔThr measurements, each consisting of $n \geq 20$ *F-D* curves. *p* values were calculated with the Mann-Whitney statistical test and are indicated in the figure.

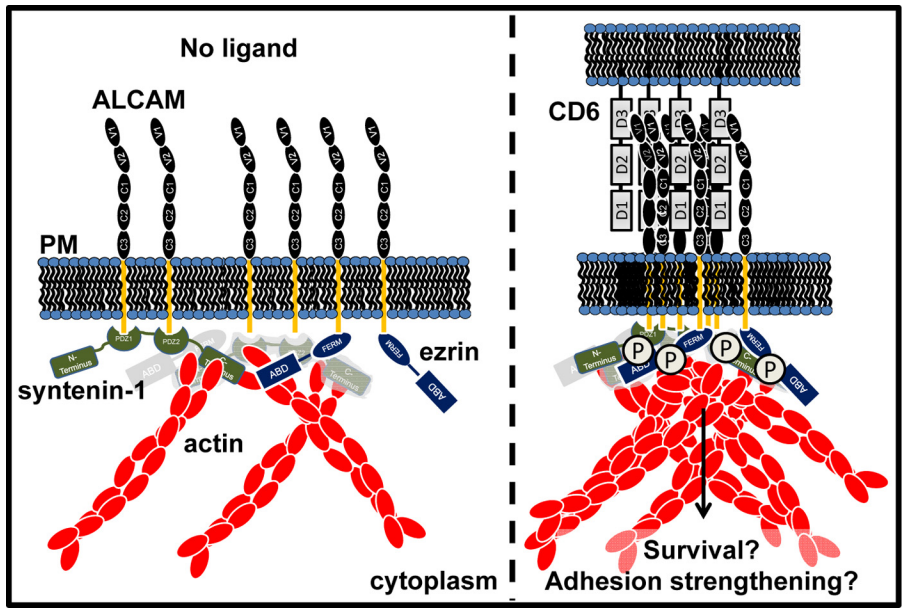

FIGURE 9. **Model of the supramolecular complex formed during ALCAM-CD6-mediated adhesion.** When ALCAM binds CD6, a supramolecular complex is formed with the adaptor proteins ezrin and syntenin-1 coupling the cytoplasmic tail of ALCAM to actin. Syntenin-1 binds the PDZ-binding motif at the C terminus of the cytoplasmic tail and tightens the bonds by coupling ALCAM to the actin cortex. Ezrin also connects some of the ALCAM molecules at a juxtamembrane site to actin. Upon binding of ALCAM to its ligand CD6, the complex is tightened and syntenin-1 as well as ezrin could be phosphorylated leading to outside-in signaling and ultimate cellular responses. *PM,* plasma membrane.

pressing cells (Fig. 8*E*). This suggests that the specific additional recruitment of syntenin-1 to the cytoplasmic tail of ALCAM strengthens and stabilizes binding to the ligand CD6.

DISCUSSION

This study combines FRET-FLIM measurements with single-cell force spectroscopy and co-IPs to demonstrate that in resting cells in the absence of active cell adhesion the transmembrane protein ALCAM is pre-organized in a supramolecular complex consisting of syntenin-1, ezrin, and actin. Binding of ALCAM to its ligand CD6 further strengthens and augments these interactions (Fig. 9). Finally, binding of syntenin-1 to the ALCAM cytoplasmic tail appears to be crucial to maintain the integrity of the complex and to mediate strong adhesion to the ligand CD6. Because the heterotypic ALCAM-CD6 interaction has been shown to play an important role in the formation and strengthening of the immunological synapse, our study provides for the first time insights into the molecular players in a strong adhesive complex formed at the DC side of the synapse that could contribute to stabilize the DC-T cell contact.

Although interactions between ALCAM and actin have already been demonstrated (18, 19, 26), nothing was known about the intracellular partners physically mediating the interaction between the actin cytoskeleton and the cytoplasmic tail of ALCAM. Interactions with ezrin most likely represent the molecular link between ALCAM and the cytoskeleton. Co-immunoprecipitation shows that ezrin binds to ALCAM. The capacity of ezrin to bind to PDZ-containing proteins, such as EBP50 (47), opens the possibility that binding to ALCAM could occur via syntenin-1 or a yet unknown partner. A known cytoplasmic interactor of ALCAM is protein kinase Cα (PKCα), which our laboratory previously demonstrated to play a role in cytoskeleton-dependent avidity modulation of homo- and heterotypic ALCAM-mediated adhesion (19). However, the cytoplasmic tail of ALCAM is not a direct target for PKCα, because it is not phosphorylated after PKC activation, and it does not contain conserved PKC phosphorylation motifs (19). Because PKC can influence ERM protein activities, both by altering their conformation and by determining the binding capacity of their interaction partners (48), it is tempting to speculate that ezrin could be the direct target for PKCα at these ALCAM supramolecular complexes. Recent work from Hwangbo *et al.* (49) demonstrated that syntenin-1 also mediates adhesion-induced activation of PKCα in human breast cancer and melanoma cells, suggesting the existence of a possible interplay between PKCα, syntenin-1, and ezrin at the ALCAM supramolecular complex.

Furthermore, a spatiotemporal regulatory role for syntenin-1 in actin remodeling has also been documented in CD4 T cells during HIV-1 binding and entry (50). By single-cell force spectroscopy, we have here demonstrated that the interaction with syntenin-1 is strictly dependent on Thr residues in the cytoplasmic tail of ALCAM. Previous work from our laboratory showed no difference between cells expressing ALCAM wild type and cells expressing the ALCAM-ΔThr mutant in the ability to attach to ALCAM-coated plates (19), thus in apparent contrast to the single-cell force spectroscopy measurements reported here. However, this discrepancy can be reconciled by the fact that, with respect to a static plate adhesion assay, single-cell force spectroscopy better mimics the dynamic interactions occurring between cells and ligand (51, 52) and is therefore better suited to pinpoint subtle differences in adhesion strength of short lived interactions under force/stress. Recognition of C-terminal motifs appears to be the dominant mode of PDZ-ligand interaction; however, binding to non-C-terminal "internal" motifs has also been reported in the literature (53, 54). This

could explain why the GFP tag fused at the C terminus of ALCAM did not affect the interaction of the PDZ-binding motif in the ALCAM tail with syntenin-1.

Another player that might have a role in regulating the interaction of ALCAM with cytoskeletal component is the tetraspanin CD9 that was reported to directly interact with ALCAM at the cell surface of T cells, thereby enhancing ALCAM function by augmented clustering of ALCAM molecules and up-regulation of ALCAM surface expression (55). In fact, CD9 has been shown to be part of a tetraspanin web that is directly linked to ERM proteins (56) and to modulate the composition of adhesive complexes influencing the presence of integrins, actin, and actin-binding proteins at sites of cell adhesion and matrix assembly (57). CD9 could therefore play a yet unrecognized role on organizing the ALCAM supramolecular assembly.

This study is one of the few addressing the players of the immunological synapse at the DC side. We confirmed that human DCs express ALCAM as well as syntenin-1 and ezrin, which corresponds with RNA expression data (58). In fact, although an abundance of information is available about the receptors and their dynamics at the surface of the T cell, including the involvement of syntenin-1 in T cell polarization (59), very little is known about the biochemical signals transduced into the interacting DC. In fact, the DC side of the immunological synapse has been reported to have an anti-apoptotic function to keep the DC alive and fit as long as possible to increase the chance of effective encounters with T cells (60). Moreover, Al-Alwan *et al.* (61, 62) demonstrated that the DC cytoskeleton does not play a passive role in the formation of the immunological synapse but is rather actively polarized upon MHC class II ligation and critical for proper T cell activation. The engagement of ALCAM with CD6 on the T cells could therefore contribute to this process by allowing the formation of a stable nucleation site for further actin polymerization to strengthen the cell-cell interaction. In addition, in T cells ezrin has been shown to be a negative regulator of death receptor-induced apoptosis (63). The enrichment of ezrin in the ALCAM supramolecular assembly at the DC side could provide another survival signal to the DCs.

This study contributes to increasing our understanding of the DC-associated molecular players involved in the mechanical strengthening of the contact with T cells, which might provide novel insights into regulatory mechanisms of DC function.

Acknowledgments—We thank all members of our laboratories for encouragement and constructive criticisms. We acknowledge Christian Blum for help with time-correlated single photon-counting fluorescence lifetime measurements. We thank Pascale Zimmermann for the plasmids for syntenin-1-GFP and syntenin-1-mCherry and Satyajit Mayor for the plasmids for ezrin-GFP and ezrin-RFP. We also thank Theodorus W. J. Gadella and Joachim Goedhart (Molecular Cytology, University of Amsterdam) for the pmTurquoise2-N1 and mVenus (L68V)-mTurquoise2 plasmids. We thank Ruurd Torensma for providing the AZN-L50 antibody. The atomic force microscope was supported by Netherlands Organization for Scientific Research Medium Sized Investment Grant 91110007.

REFERENCES

1. Bowen, M. A., Patel, D. D., Li, X., Modrell, B., Malacko, A. R., Wang, W. C., Marquardt, H., Neubauer, M., Pesando, J. M., and Francke, U. (1995) Cloning, mapping, and characterization of activated leukocyte-cell adhesion molecule (ALCAM), a CD6 ligand. *J. Exp. Med.* **181,** 2213–2220
2. Levesque, M. C., Heinly, C. S., Whichard, L. P., and Patel, D. D. (1998) Cytokine-regulated expression of activated leukocyte cell adhesion molecule (CD166) on monocyte-lineage cells and in rheumatoid arthritis synovium. *Arthritis Rheum.* **41,** 2221–2229
3. Cortés, F., Deschaseaux, F., Uchida, N., Labastie, M. C., Friera, A. M., He, D., Charbord, P., and Péault, B. (1999) HCA, an immunoglobulin-like adhesion molecule present on the earliest human hematopoietic precursor cells, is also expressed by stromal cells in blood-forming tissues. *Blood* **93,** 826–837
4. Nelissen, J. M., Torensma, R., Pluyter, M., Adema, G. J., Raymakers, R. A., van Kooyk, Y., and Figdor, C. G. (2000) Molecular analysis of the hematopoiesis supporting osteoblastic cell line U2-OS. *Exp. Hematol.* **28,** 422–432
5. Uchida, N., Yang, Z., Combs, J., Pourquié, O., Nguyen, M., Ramanathan, R., Fu, J., Welply, A., Chen, S., Weddell, G., Sharma, A. K., Leiby, K. R., Karagogeos, D., Hill, B., Humeau, L., Stallcup, W. B., Hoffman, R., Tsukamoto, A. S., Gearing, D. P., and Péault, B. (1997) The characterization, molecular cloning, and expression of a novel hematopoietic cell antigen from CD34+ human bone marrow cells. *Blood* **89,** 2706–2716
6. Ohneda, O., Ohneda, K., Arai, F., Lee, J., Miyamoto, T., Fukushima, Y., Dowbenko, D., Lasky, L. A., and Suda, T. (2001) ALCAM (CD166): its role in hematopoietic and endothelial development. *Blood* **98,** 2134–2142
7. Tanaka, H., Matsui, T., Agata, A., Tomura, M., Kubota, I., McFarland, K. C., Kohr, B., Lee, A., Phillips, H. S., and Shelton, D. L. (1991) Molecular cloning and expression of a novel adhesion molecule, SC1. *Neuron* **7,** 535–545
8. Stephan, J. P., Bald, L., Roberts, P. E., Lee, J., Gu, Q., and Mather, J. P. (1999) Distribution and function of the adhesion molecule BEN during rat development. *Dev. Biol.* **212,** 264–277
9. Bruder, S. P., Ricalton, N. S., Boynton, R. E., Connolly, T. J., Jaiswal, N., Zaia, J., and Barry, F. P. (1998) Mesenchymal stem cell surface antigen SB-10 corresponds to activated leukocyte cell adhesion molecule and is involved in osteogenic differentiation. *J. Bone Miner. Res.* **13,** 655–663
10. Tomita, K., van Bokhoven, A., Jansen, C. F., Kiemeney, L. A., Karthaus, H. F., Vriesema, J., Bussemakers, M. J., Witjes, J. A., and Schalken, J. A. (2003) Activated leukocyte cell adhesion molecule (ALCAM) expression is associated with a poor prognosis for bladder cancer patients. *Uro Oncol.* **3,** 121–129
11. King, J. A., Ofori-Acquah, S. F., Stevens, T., Al-Mehdi, A. B., Fodstad, O., and Jiang, W. G. (2004) Activated leukocyte cell adhesion molecule in breast cancer: prognostic indicator. *Breast Cancer Res.* **6,** R478–R487
12. Ihnen, M., Wirtz, R. M., Kalogeras, K. T., Milde-Langosch, K., Schmidt, M., Witzel, I., Eleftheraki, A. G., Papadimitriou, C., Jänicke, F., Briassoulis, E., Pectasides, D., Rody, A., Fountzilas, G., and Müller, V. (2010) Combination of osteopontin and activated leukocyte cell adhesion molecule as potent prognostic discriminators in HER2- and ER-negative breast cancer. *Br. J. Cancer* **103,** 1048–1056
13. Weichert, W., Knösel, T., Bellach, J., Dietel, M., and Kristiansen, G. (2004) ALCAM/CD166 is overexpressed in colorectal carcinoma and correlates with shortened patient survival. *J. Clin. Pathol.* **57,** 1160–1164
14. van Kempen, L. C., Nelissen, J. M., Degen, W. G., Torensma, R., Weidle, U. H., Bloemers, H. P., Figdor, C. G., and Swart, G. W. (2001) Molecular basis for the homophilic activated leukocyte cell adhesion molecule (ALCAM)-ALCAM interaction. *J. Biol. Chem.* **276,** 25783–25790
15. Lunter, P. C., van Kilsdonk, J. W., van Beek, H., Cornelissen, I. M., Bergers, M., Willems, P. H., van Muijen, G. N., and Swart, G. W. (2005) Activated leukocyte cell adhesion molecule (ALCAM/CD166/MEMD), a novel actor in invasive growth, controls matrix metalloproteinase activity. *Cancer Res.* **65,** 8801–8808
16. Weidle, U. H., Eggle, D., Klostermann, S., and Swart, G. W. (2010) ALCAM/CD166: cancer-related issues. *Cancer Genomics Proteomics* **7,** 231–243

17. Kijima, N., Hosen, N., Kagawa, N., Hashimoto, N., Nakano, A., Fujimoto, Y., Kinoshita, M., Sugiyama, H., and Yoshimine, T. (2012) CD166/activated leukocyte cell adhesion molecule is expressed on glioblastoma progenitor cells and involved in the regulation of tumor cell invasion. *Neuro. Oncol.* **14,** 1254–1264
18. Nelissen, J. M., Peters, I. M., de Grooth, B. G., van Kooyk, Y., and Figdor, C. G. (2000) Dynamic regulation of activated leukocyte cell adhesion molecule-mediated homotypic cell adhesion through the actin cytoskeleton. *Mol. Biol. Cell* **11,** 2057–2068
19. Zimmerman, A. W., Nelissen, J. M., van Emst-de Vries, S. E., Willems, P. H., de Lange, F., Collard, J. G., van Leeuwen, F. N., and Figdor, C. G. (2004) Cytoskeletal restraints regulate homotypic ALCAM-mediated adhesion through PKCα independently of Rho-like GTPases. *J. Cell Sci.* **117,** 2841–2852
20. Hassan, N. J., Barclay, A. N., and Brown, M. H. (2004) Frontline: optimal T cell activation requires the engagement of CD6 and CD166. *Eur. J. Immunol.* **34,** 930–940
21. Grakoui, A., Bromley, S. K., Sumen, C., Davis, M. M., Shaw, A. S., Allen, P. M., and Dustin, M. L. (1999) The immunological synapse: a molecular machine controlling T cell activation. *Science* **285,** 221–227
22. Gimferrer, I., Ibáñez, A., Farnós, M., Sarrias, M. R., Fenutría, R., Roselló, S., Zimmermann, P., David, G., Vives, J., Serra-Pagès, C., and Lozano, F. (2005) The lymphocyte receptor CD6 interacts with syntenin-1, a scaffolding protein containing PDZ domains. *J. Immunol.* **175,** 1406–1414
23. Cayrol, R., Wosik, K., Berard, J. L., Dodelet-Devillers, A., Ifergan, I., Kebir, H., Haqqani, A. S., Kreymborg, K., Krug, S., Moumdjian, R., Bouthillier, A., Becher, B., Arbour, N., David, S., Stanimirovic, D., and Prat, A. (2008) Activated leukocyte cell adhesion molecule promotes leukocyte trafficking into the central nervous system. *Nat. Immunol.* **9,** 137–145
24. Zimmerman, A. W., Joosten, B., Torensma, R., Parnes, J. R., van Leeuwen, F. N., and Figdor, C. G. (2006) Long-term engagement of CD6 and ALCAM is essential for T-cell proliferation induced by dendritic cells. *Blood* **107,** 3212–3220
25. Mempel, T. R., Henrickson, S. E., and Von Andrian, U. H. (2004) T-cell priming by dendritic cells in lymph nodes occurs in three distinct phases. *Nature* **427,** 154–159
26. Te Riet, J., Zimmerman, A. W., Cambi, A., Joosten, B., Speller, S., Torensma, R., van Leeuwen, F. N., Figdor, C. G., and de Lange, F. (2007) Distinct kinetic and mechanical properties govern ALCAM-mediated interactions as shown by single-molecule force spectroscopy. *J. Cell Sci.* **120,** 3965–3976
27. Burkhardt, J. K., Carrizosa, E., and Shaffer, M. H. (2008) The actin cytoskeleton in T cell activation. *Annu. Rev. Immunol.* **26,** 233–259
28. Jares-Erijman, E. A., and Jovin, T. M. (2006) Imaging molecular interactions in living cells by FRET microscopy. *Curr. Opin. Chem. Biol.* **10,** 409–416
29. Wouters, F. S., Verveer, P. J., and Bastiaens, P. I. (2001) Imaging biochemistry inside cells. *Trends Cell Biol.* **11,** 203–211
30. Hoppe, A., Christensen, K., and Swanson, J. A. (2002) Fluorescence resonance energy transfer-based stoichiometry in living cells. *Biophys. J.* **83,** 3652–3664
31. Emiliani, V., Sanvitto, D., Tramier, M., Piolot, T., Petrasek, Z., Kemnitz, K., Durieux, C., and Coppey-Moisan, M. (2003) Low-intensity two-dimensional imaging of fluorescence lifetimes in living cells. *Appl. Phys. Lett.* **83,** 2471
32. Bücherl, C., Aker, J., de Vries, S., and Borst, J. W. (2010) Probing protein-protein interactions with FRET-FLIM. *Methods Mol. Biol.* **655,** 389–399
33. Fehon, R. G., McClatchey, A. I., and Bretscher, A. (2010) Organizing the cell cortex: the role of ERM proteins. *Nat. Rev. Mol. Cell Biol.* **11,** 276–287
34. Yonemura, S., Hirao, M., Doi, Y., Takahashi, N., Kondo, T., Tsukita, S., and Tsukita, S. (1998) Ezrin/radixin/moesin (ERM) proteins bind to a positively charged amino acid cluster in the juxta-membrane cytoplasmic domain of CD44, CD43, and ICAM-2. *J. Cell Biol.* **140,** 885–895
35. Barreiro, O., Yanez-Mo, M., Serrador, J. M., Montoya, M. C., Vicente-Manzanares, M., Tejedor, R., Furthmayr, H., and Sanchez-Madrid, F. (2002) Dynamic interaction of VCAM-1 and ICAM-1 with moesin and ezrin in a novel endothelial docking structure for adherent leukocytes. *J. Cell Biol.* **157,** 1233–1245
36. Gallardo, R., Ivarsson, Y., Schymkowitz, J., Rousseau, F., and Zimmermann, P. (2010) Structural diversity of PDZ-lipid interactions. *Chembiochem* **11,** 456–467
37. Grootjans, J. J., Zimmermann, P., Reekmans, G., Smets, A., Degeest, G., Dürr, J., and David, G. (1997) Syntenin, a PDZ protein that binds syndecan cytoplasmic domains. *Proc. Natl. Acad. Sci. U.S.A.* **94,** 13683–13688
38. Goswami, D., Gowrishankar, K., Bilgrami, S., Ghosh, S., Raghupathy, R., Chadda, R., Vishwakarma, R., Rao, M., and Mayor, S. (2008) Nanoclusters of GPI-anchored proteins are formed by cortical actin-driven activity. *Cell* **135,** 1085–1097
39. Goedhart, J., von Stetten, D., Noirclerc-Savoye, M., Lelimousin, M., Joosen, L., Hink, M. A., van Weeren, L., Gadella, T. W., Jr., and Royant, A. (2012) Structure-guided evolution of cyan fluorescent proteins towards a quantum yield of 93%. *Nat. Commun.* **3,** 751
40. Schlachter, S., Elder, A. D., Esposito, A., Kaminski, G. S., Frank, J. H., van Geest, L. K., and Kaminski, C. F. (2009) mhFLIM: resolution of heterogeneous fluorescence decays in widefield lifetime microscopy. *Opt. Express* **17,** 1557–1570
41. Cambi, A., Joosten, B., Koopman, M., de Lange, F., Beeren, I., Torensma, R., Fransen, J. A., Garcia-Parajó, M., van Leeuwen, F. N., and Figdor, C. G. (2006) Organization of the integrin LFA-1 in nanoclusters regulates its activity. *Mol. Biol. Cell* **17,** 4270–4281
42. Bolte, S., and Cordelières, F. P. (2006) A guided tour into subcellular colocalization analysis in light microscopy. *J. Microsc.* **224,** 213–232
43. Friedrichs, J., Helenius, J., and Muller, D. J. (2010) Quantifying cellular adhesion to extracellular matrix components by single-cell force spectroscopy. *Nat. Protoc.* **5,** 1353–1361
44. Lamers, E., te Riet, J., Domanski, M., Luttge, R., Figdor, C. G., Gardeniers, J. G., Walboomers, X. F., and Jansen, J. A. (2012) Dynamic cell adhesion and migration on nanoscale grooved substrates. *Eur. Cell. Mater.* **23,** 182–193
45. te Riet, J., Katan, A. J., Rankl, C., Stahl, S. W., van Buul, A. M., Phang, I. Y., Gomez-Casado, A., Schön, P., Gerritsen, J. W., Cambi, A., Rowan, A. E., Vancso, G. J., Jonkheijm, P., Huskens, J., Oosterkamp, T. H., Gaub, H., Hinterdorfer, P., Figdor, C. G., and Speller, S. (2011) Interlaboratory round robin on cantilever calibration for AFM force spectroscopy. *Ultramicroscopy* **111,** 1659–1669
46. Beekman, J. M., and Coffer, P. J. (2008) The ins and outs of syntenin, a multifunctional intracellular adaptor protein. *J. Cell Sci.* **121,** 1349–1355
47. Reczek, D., Berryman, M., and Bretscher, A. (1997) Identification of EBP50: a PDZ-containing phosphoprotein that associates with members of the ezrin-radixin-moesin family. *J. Cell Biol.* **139,** 169–179
48. Larsson, C. (2006) Protein kinase C and the regulation of the actin cytoskeleton. *Cell. Signal.* **18,** 276–284
49. Hwangbo, C., Kim, J., Lee, J. J., and Lee, J. H. (2010) Activation of the integrin effector kinase focal adhesion kinase in cancer cells is regulated by crosstalk between protein kinase Cα and the PDZ adapter protein mda-9/Syntenin. *Cancer Res.* **70,** 1645–1655
50. Gordón-Alonso, M., Rocha-Perugini, V., Álvarez, S., Moreno-Gonzalo, O., Ursa, A., López-Martín, S., Izquierdo-Useros, N., Martínez-Picado, J., Muñoz-Fernández, M. Á., Yáñez-Mó, M., and Sánchez-Madrid, F. (2012) The PDZ-adaptor protein syntenin-1 regulates HIV-1 entry. *Mol. Biol. Cell* **23,** 2253–2263
51. Müller, D. J., Helenius, J., Alsteens, D., and Dufrêne, Y. F. (2009) Force probing surfaces of living cells to molecular resolution. *Nat. Chem. Biol.* **5,** 383–390
52. Te Riet, J., Helenius, J., Strohmeyer, N., Cambi, A., Figdor, C. G., and Muller, D. J. (2014) Dynamic coupling of ALCAM to the actin cortex strengthens cell adhesion to CD6. *J. Cell Sci.* **127,** 1595–1606
53. London, T. B., Lee, H. J., Shao, Y., and Zheng, J. (2004) Interaction between the internal motif KT*XXX*I of Idax and mDvl PDZ domain. *Biochem. Biophys. Res. Commun.* **322,** 326–332
54. Penkert, R. R., DiVittorio, H. M., and Prehoda, K. E. (2004) Internal recognition through PDZ domain plasticity in the Par-6-Pals1 complex. *Nat. Struct. Mol. Biol.* **11,** 1122–1127
55. Gilsanz, A., Sánchez-Martín, L., Gutiérrez-López, M. D., Ovalle, S., Machado-Pineda, Y., Reyes, R., Swart, G. W., Figdor, C. G., Lafuente, E. M., and Cabañas, C. (2013) ALCAM/CD166 adhesive function is regulated by

the tetraspanin CD9. *Cell. Mol. Life Sci.* **70,** 475–493
56. Sala-Valdés, M., Ursa, A., Charrin, S., Rubinstein, E., Hemler, M. E., Sánchez-Madrid, F., and Yáñez-Mó, M. (2006) EWI-2 and EWI-F link the tetraspanin web to the actin cytoskeleton through their direct association with ezrin-radixin-moesin proteins. *J. Biol. Chem.* **281,** 19665–19675
57. Cook, G. A., Longhurst, C. M., Grgurevich, S., Cholera, S., Crossno, J. T., Jr., and Jennings, L. K. (2002) Identification of CD9 extracellular domains important in regulation of CHO cell adhesion to fibronectin and fibronectin pericellular matrix assembly. *Blood* **100,** 4502–4511
58. Buschow, S. I., Lasonder, E., van Deutekom, H. W., Oud, M. M., Beltrame, L., Huynen, M. A., de Vries, I. J., Figdor, C. G., and Cavalieri, D. (2010) Dominant processes during human dendritic cell maturation revealed by integration of proteome and transcriptome at the pathway level. *J. Proteome Res.* **9,** 1727–1737
59. Sala-Valdés, M., Gordón-Alonso, M., Tejera, E., Ibáñez, A., Cabrero, J. R., Ursa, A., Mittelbrunn, M., Lozano, F., Sánchez-Madrid, F., and Yáñez-Mó, M. (2012) Association of syntenin-1 with M-RIP polarizes Rac-1 activation during chemotaxis and immune interactions. *J. Cell Sci.* **125,** 1235–1246
60. Riol-Blanco, L., Delgado-Martín, C., Sánchez-Sánchez, N., Alonso-C, L. M., Gutiérrez-López, M. D., Del Hoyo, G. M., Navarro, J., Sánchez-Madrid, F., Cabañas, C., Sánchez-Mateos, P., and Rodríguez-Fernández, J. L. (2009) Immunological synapse formation inhibits, via NF-kappaB and FOXO1, the apoptosis of dendritic cells. *Nat. Immunol.* **10,** 753–760
61. Al-Alwan, M. M., Liwski, R. S., Haeryfar, S. M., Baldridge, W. H., Hoskin, D. W., Rowden, G., and West, K. A. (2003) Cutting edge: dendritic cell actin cytoskeletal polarization during immunological synapse formation is highly antigen-dependent. *J. Immunol.* **171,** 4479–4483
62. Al-Alwan, M. M., Rowden, G., Lee, T. D., and West, K. A. (2001) The dendritic cell cytoskeleton is critical for the formation of the immunological synapse. *J. Immunol.* **166,** 1452–1456
63. Kuo, W. C., Yang, K. T., Hsieh, S. L., and Lai, M. Z. (2010) Ezrin is a negative regulator of death receptor-induced apoptosis. *Oncogene* **29,** 1374–1383

Syntenin-1 and Ezrin Proteins Link Activated Leukocyte Cell Adhesion Molecule to the Actin Cytoskeleton

Cicerone Tudor, Joost te Riet, Christina Eich, Rolf Harkes, Nick Smisdom, Jessica Bouhuijzen Wenger, Marcel Ameloot, Matthew Holt, Johannes S. Kanger, Carl G. Figdor, Alessandra Cambi and Vinod Subramaniam

J. Biol. Chem. 2014, 289:13445-13460.
doi: 10.1074/jbc.M113.546754 originally published online March 24, 2014
